ACS APPLIED MATERIALS & INTERFACES

Research Article

www.acsami.org

Affinity of the Interface between Hydroxyapatite (0001) and Titanium (0001) Surfaces: A First-Principles Investigation

Jin P. Sun,[†] Jianhong Dai,[†] Yan Song,*[,†] You Wang,[‡] and Rui Yang[§]

[†]School of Materials Science and Engineering, Harbin Institute of Technology at Weihai, 2 West Wenhua Road, Weihai 264209, China

[‡]School of Materials Science and Engineering, Harbin Institute of Technology, 92 West Da-Zhi Street, Harbin 150001, China

[§]Institute of Metal Research, Chinese Academy of Sciences, 72 Wenhua Road, Shenyang 110016, China

Supporting Information

ABSTRACT: A basic understanding of the affinity between the hydroxyapatite (HA) and α-Ti surfaces is obtained through electronic structure calculations by first-principles method. The surface energies of HA(0001), HA ($01\bar{1}0$), HA ($10\bar{1}1$), and Ti(0001) surfaces have been calculated. The HA(0001) presents the most thermodynamically stable of HA. The HA/Ti interfaces were constructed by two kinds of interface models, the single interface (denoted as SI) and the double-interface (denoted as DI). Two methods, the full relaxation and the UBER, were applied to determine the interfacial separation and the atomic arrangement in the interfacial zone. The works of adhesion of interfaces with various stoichiometric HA surfaces were evaluated. For the HA(0001)/Ti(0001) interfaces, the work of adhesion is strongly dependent on the chemical environment of the HA surface. The values are −2.33, −1.52, and −0.80 J/m^2 for the none-, single-, and double-Ca terminated HA/Ti interfaces, respectively. The influence of atomic relaxation on the work of adhesion and interface separation is discussed. Full relaxation results include −1.99 J/m^2 work of adhesion and 0.220 nm separation between HA and Ti for the DI of 1-Ca-HA/Ti interface, while they are −1.14 J/m^2 and 0.235 nm by partial relaxation. Analysis of electronic structure reveals that charge transfer between HA and Ti slabs occurs during the formation of the HA/Ti interface. The transfer generates the Ti−O or Ti−Ca bonds across the interface and drives the HA/Ti interface system to metallic characteristic. The energetically favorable interfaces are formed when the outmost layer of HA comprises more O atoms at the interface.

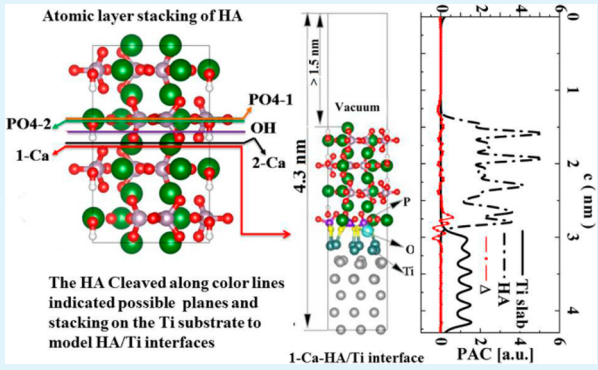

KEYWORDS: *hydroxyapatite, HA/Ti interface, work of adhesion, first-principles*

1. INTRODUCTION

Hydroxyapatite [$Ca_{10}(PO_4)_6(OH)_2$, HA] is extensively used for bioactive coatings due to its chemical similarity to bone and teeth.[1−3] Titanium and its alloys have been greatly applied as implant metals due to their inert properties and biocompatibility. HA-coated Ti alloy implants show excellent biocompatibility and satisfactory mechanical properties during short-term implant-to-bone fixation. However, inherent defects of coating structure, such as great differences of physical properties and the low adhesion strength between HA coating and Ti matrix, low interface shear strength, coating stripping, cracks on the interface, and particle pieces limit their long-term performance.[4,5] The critical factor to extend the lifetime of titanium alloys as implants is to strengthen adhesion between HA and Ti surfaces. Thus, it is essential to study the affinity of HA/Ti interface at the electronic level. Therefore, a detailed theoretical analysis of HA/Ti interface will be of significant interest.

There are some guidelines to improve the adhesion between HA and Ti alloys: (1) denser microstructure and thinner HA coatings resulting in high bonding strength,[6,7] (2) overcoming the stress concentration and improving cohesive strength among interlamellar structure, (3) doping with other elements such as Y, C, Sr, and Ag in HA crystals,[6,8−10] (4) controlling surface texture and compositions of material.[11,12] Recently, Carradó[13] investigated the plasma-sprayed HA coating on titanium alloys. No impurity phase was found in the microstructure, but different stress states were shown in two sides of the interface. Microcracks were present along the coating-substrate interface. Roy et al.[9] studied the mechanical properties of plasma-sprayed and silver-doped HA coatings. The coatings show a pure adhesive failure indicating a strong bonding between the HA coating and the Ti substrate. New techniques were developed to produce the thinner, denser, and higher crystalline HA ration coatings on metallic substrates.[6,8]

Received: July 22, 2014
Accepted: November 12, 2014
Published: November 12, 2014

Table 1. Calculated Lattice Parameters (in nm) and Elastic Constants (in GPa) of Bulk HA and α-Ti

	lattice params		elastic constants				
	a	c	C_{11}	C_{12}	C_{13}	C_{33}	C_{44}
HA[a]							
present	0.9349	0.6821	137.2	44.5	57.8	164.8	42.3
exptl	0.9408	0.6891	137, 115	42.5, 42.2	54.9, 30.0	172, 125	39.6, 22.8
calcd	0.9362	0.6869	126.4, 140	35.6, 42.2	65.1, 55.6	167.4, 174.8	44.3, 47.5
Ti[b]							
present	0.292	0.463	192.1	90.5	89.4	197.3	40.7
exptl	0.295	0.468	162.4	92	69	180.7	46.7
calcd	0.2919	0.4621	193	72	85	188	40

[a]Experimental and other theoretical calculated lattice parameters are from refs 31 and 32; elastic constants are from refs 31 and 37 (exptl) and from refs 38 and 39 (calcd). [b]Experimental lattice parameters and elastic constants are from refs 33 and 36, and other theoretical calculated values are from ref 34.

Wei et al.[6] reported that well-crystallized and strong adhesive strength of HA films were produced via hydrothermal crystal growth onto Ti substrate with HA seed crystal layer. However, none of these experimental studies reveals the morphology-bonding at atomic and electronic scale. Currently, the developments of experimental techniques enable us to analyze the structural information insight into three protein domains but still cannot distinguish single atom in contact with the surface.[14]

Since adhesion is governed by chemical bonding and mechanical interlocking, the problem is the electronic properties of the interface between the HA coating and the metal substrate. Therefore, a thorough understanding of the electronic properties of HA/Ti interfaces is of scientific interest. First-principles calculations provide a suitable means to gain the insight in understanding the physical and chemical properties of surfaces and interfaces. The methodology and reliability of such computations have been well-studied.[15,16] Canepa et al. studied the structures, vibrational frequencies, and interaction energies of formic and alendronic acids with HA(0001) and $(10\bar{1}0)$ surfaces.[15] The interactions between polylactide acids and one type of deficient HA,[17] the adsorption of lysine on HA $(10\bar{1}0)$ surface,[18] and the adsorption of glycine, proline, and hydroxyproline on the HA(0001) surface[19] were calculated. These adsorptions are mainly stabilized by the Ca−O ionic bonding, followed by hydrogen bond and/or van de Waals interaction between phosphate and O atoms, and between adsorption molecule and HA.[15,20−22] Chiatti et al.[23] investigated the feature of the ferroelectric HA(0001) surface and found that the ferroelectric OH^- alignment does not compromise the stability of the HA(0001) surface. The counterpolarization of the electronic density of the Ca^{2+} and PO_4^{3-} moieties surrounds the monodimensional OH^- polar arrays.

The first-principles investigation of HA/Ti is helpful to further understand the role of the HA/Ti interface underlying the composite mechanical properties. However, according to our knowledge, it is still lacking in the previous literature. Thus, the work of adhesion, interface energy, and electronic structures of HA(0001)/Ti(0001) are studied in this paper by first-principles method. The rest of this paper is organized as follows. We first report theoretical results for the bulk materials, including lattice parameters and elastic tensors. In the next step, we describe the determination of interfacial separation and atomic arrangement in the interfacial zone by two methods, the full relaxation and the universal binding energy relation (UBER) curves.[24] Then, the optimized interface structures are presented along with their work separation and interface energy. Finally, we investigate electronic structure and bonding of the HA/Ti interface.

2. METHODS OF CALCULATION

Calculations were performed with Vienna *ab initio* simulation package (VASP).[25,26] The generalized gradient approximation (GGA) was used for electron exchange-correlation, while the projector-augmented wave (PAW) method was used to describe the interaction between ions and electrons.[27] The 1s, $2s^22p^4$, $3s^23p^3$, $3p^64s^2d^{0.01}$, and $4s^23d^2$ were regarded as valence electron of H, O, P, Ca, and Ti, respectively. A plane-wave cutoff of 450 eV and a Gaussian smearing method with an energy broadening of 0.2 eV were used in all calculations. The ionic positions were relaxed using the conjugate gradient method for surface and interface models. The criteria for self-consistency of energy and forces were less than 0.01 eV/unit cell and 0.002 eV/nm, respectively. A 3 × 3 × 1 Γ-centered *k*-point grid was used in the relaxation of the HA(0001)/Ti(0001) interfaces, while 4 × 4 × 1 grids were used for final energy and density of states calculation. The atomic structures and electronic structures in this work were visualized by the VESTA 3 software program.[28]

3. RESULTS AND DISCUSSION

3.1. Bulk Materials. Hydroxyapatite has two different structures, the monoclinic (space group $P2_1/b$) and hexagonal. The former only occurs in the stoichiometric environment, while the latter is frequently present experimentally. Because the prepared HA coatings on the substrate of Ti often occurred in Ca-deficient states and doped with other elements, such as Y, C, Sr, and Ag,[6,8−10] therefore, the hexagonal structure is considered in this work for both bulk and HA/Ti surfaces.

The symmetry of hexagonal HA is $P6_3/m$ space group with lattice parameters a = 0.9430 nm and c = 0.6881 nm.[29] During the simulations, the symmetry is reduced to $P6_3$ space group by removing the mirror plane and forcing the alignment of the hydroxyl groups to keep stoichiometric proportion with two formula units of $Ca_5(PO_4)_3OH$ per unit cell. The crystallographic parameters of HA and α-Ti are summarized in Table 1. The optimized lattice parameters of HA are a = 0.9349 nm and c = 0.6821 nm, which are in good agreement with measurements[30−32] with the largest difference less than 0.9%. The calculated bulk lattice parameters of α-Ti also matched well the known experimental[33] and theoretical results.[34] The elastic constants of bulk HA and α-Ti are also calculated utilizing the same method as our earlier work.[35] Calculated elastic constants are listed in Table 1 together with experimental measurements[31,36,37] and other theoretical estimations.[38,39]

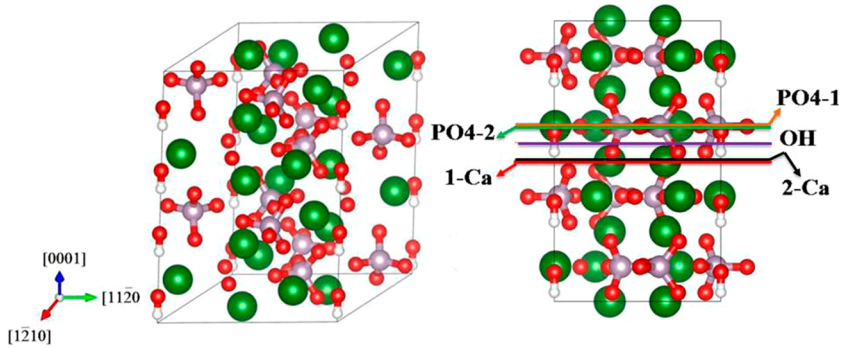

Figure 1. Atomic layer stacking of bulk HA with double unit cells. The bulk structure (left) and atomic layer stacking projected on the (10$\bar{1}$0) plane (right). Colored lines indicate possible cleavage planes. The white, red, purple, and green balls denote the H, O, P, and Ca, respectively.

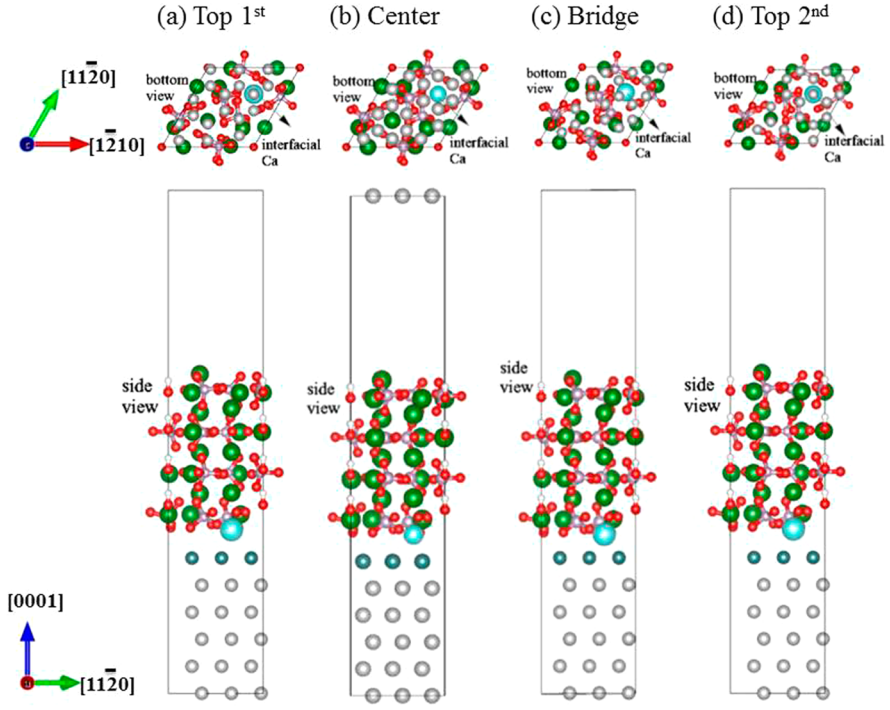

Figure 2. Bottom and side views of the four models for one Ca-terminated HA(0001)/Ti(0001) with four stacking sites: top first (a), center (b), bridge (c), and top second (d) sites. The white, red, purple, green, and light gray balls denote the H, O, P, Ca, and Ti, respectively. The bigger light-cyan ball and blue-green represents the interfacial Ca and interfacial Ti atoms, respectively.

The present elastic constants of bulk HA agree well with experimental measurements.[31,37] For α-Ti, the deviation from experimental elastic constants[36] is less than 10% except for that of C_{11} and C_{13}. The calculated C_{11} and C_{13} are in good agreement with those presented in ref 34 (also using PBE). Therefore, the bulk results on both HA and α-Ti, the crystal structure and elasticity, show reasonable correspondence to available experimental and theoretical data.

3.2. Interface Models. On the basis of the bulk lattice parameters, the optimized low index surfaces of HA and Ti (see Supporting Information), the interface models are created. This study will focus on the interface formed between the most stable and the dominant surfaces in the thermodynamic morphology,[40] viz., HA(0001) and Ti(0001), as is observed experimentally.[41,42] There is experimental evidence that crystal domains of HA films are oriented with the crystallographic *c*-axis normal to the substrate.[6,8] The other reason to select this particular interface is that it has the smallest lattice mismatch among all considered low-index surfaces of HA and α-Ti, suggesting that it is the most likely to be the most stable interface.

To identify the possible structure arrangements at the HA(0001)/Ti(0001) interface, the atomic-layer stacking along [0001] was analyzed for bulk HA and Ti. Since a two Ti atom block is the repetition unit of α-Ti stacking, there is only one kind of termination of Ti(0001) surface. The cross sections of HA and HA crystals are shown in Figure 1. The colored lines in Figure 1 indicate how we cleave our models. For example, removing particles upon the red line named 1-Ca in Figure 1 yields a one Ca atom terminated surface model, removing particles upon the 2-Ca black line yields the two Ca atoms terminated surface, and so on. For convenience, hereafter, they are referred to as 1-Ca, 2-Ca, PO_4-1, OH, and PO_4-2, each one corresponding to the crystal below one of the colored lines in Figure 1.

There are five possibilities of stacking between HA(0001) and Ti(0001). However, due to the variance of atomic densities at different surfaces, some stacking ways could be selected as a

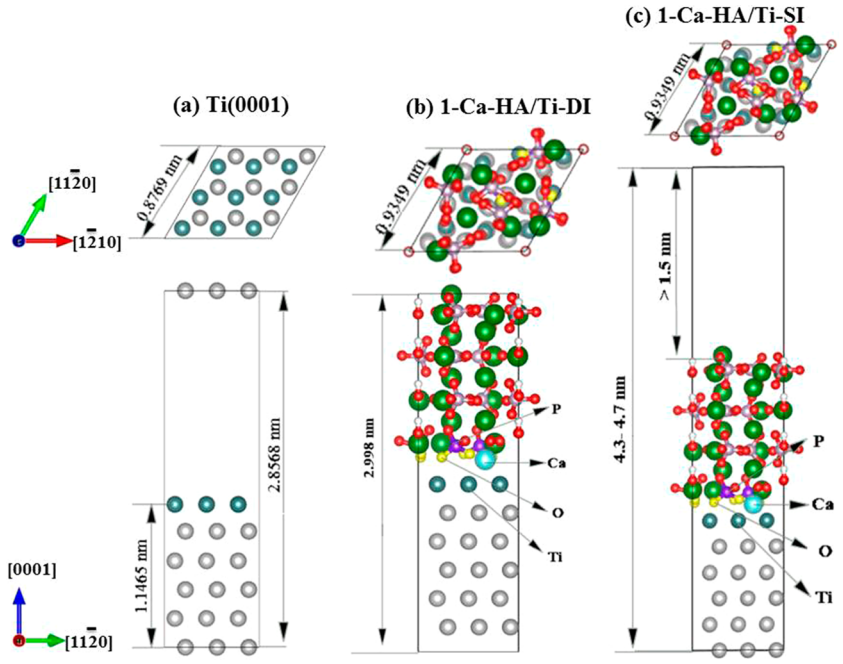

Figure 3. Top and side views of the slab models employed in the present work: (a) Ti(0001) surface, (b) HA(0001)/Ti(0001) double interfaces model, and (c) HA(0001)/Ti(0001) single interface model with more than 1.5 nm vacuum atop the upmost HA. The white, red, purple, green, and light gray balls denote the H, O, P, Ca, and Ti atoms, respectively. The nearest atoms to the interface are denoted by yellow (the O atom), light cyan (the Ca atom), dark purple (the P atom), and dark blue (the Ti atom) balls, respectively.

more stable priori. We reduce the range of considered structures to three sequences, namely, 1Ca-HA(0001)/Ti(0001), 2Ca-HA(0001)/Ti(0001), and PO_4-HA(0001)/Ti-(0001), denoted as *n*-Ca-HA/Ti (*n* = 1 or 2) and PO_4-HA/Ti. Among them, the 2-Ca-HA/Ti, with the atomic stacking at the interface as (O−O−Ca−CaⅠTi−Ti−...) metal to metal stacked, represents oxygen-poor stacking with loose coordinate. For the 1-Ca-HA/Ti case, there are four possible stacking configurations distinguished by the position of the interfacial Ca atom in HA relative to the Ti substrate (as shown in Figure 2). The interfacial Ca atom locates (a) at the top of interfacial Ti atom (denoted as top first), (b) at the center of the hexagon consisted by interfacial and subinterfacial Ti atoms (denoted as center), (c) at the bridge site of the surface Ti atoms (denoted as bridge), and (d) at the top of subinterfacial Ti atom (denoted as top second).

As the HA/Ti interface structures are modeled by HA and Ti slabs stacking into multilayers, the slabs should be sufficiently thick to remove interactions from their opposite surfaces and other finite size effects. On the other side, the increase of the number of atoms considered makes computational effort increase sharply. In this work the HA surface slab thickness is quantitative by the number of HA units and Ti atomic layers aligning along their surface normal. The convergence of surface energy with respect to slab thickness of low index surfaces of HA and Ti is detailed in Supporting Information.

For the interfacial slab, appropriate separation is needed for the original models. Thus, it is important to obtain the proper separations between the two subslabs. In this work, the dependences of total energy and adhesive energy on the interfacial separation were checked using two methods. The first one is UBER[24] described in section 3.3.1. The other method is full relaxation of the interface supercells with different interfacial separations to obtain the optimized geometrics and the optimized separation between two subslabs. The details to obtain the optimum separations between HA(0001) and Ti(0001) in the optimized geometries of HA/Ti interface are shown in section 3.3.2.

Two interface models were constructed. One is by combining (1 × 1 × 2) HA on the substrate of (3 × 3× 6) Ti stacking along the [0001] direction, thus forming sandwich-like superlattices, *i.e.*, without vacuum in the supercell (named as double-interface model, DI). The other is by stacking the (1 × 1 × 2) HA(0001) slab on the substrate of (3 × 3 × 6) Ti(0001) with more than 1.5 nm vacuum in the top of the HA(0001)/Ti (0001) interface (referred to as the single-interface model, abbreviated as SI). The size of the supercell is (3 × 3) unit cell of Ti in directions *a* and *b* and about 3.0 nm for DI or 4.3−4.7 nm for SI in the *c* direction with 142 atoms as shown in Figure 3b,c. The lattice misfit between the two subslabs of Ti(0001) and HA(0001) surfaces is about 6.2%. A large number of calculations were carried out to investigate the influence of relaxation methods and separations between HA(0001) and Ti(0001) surfaces on the physical and chemical properties of DI and SI.

3.3. Optimized Interface Structures. The convergences of surface energy with respect to the thickness were tested and shown in Supporting Information. After obtaining the supercell slabs to combine the interface, the separations between two slabs are optimized for each considered system using the above-mentioned UBER and full relaxation. In the UBER method, the static separations are obtained, in which all atoms of each slab are kept fixed to maintain the corresponding arrangement of surfaces. The relaxed separations are obtained by first-principles calculation for stoichiometric stacking (1-Ca-HA/Ti). The fully first-principles calculations are allowing all interface supercells with different interfacial separations to relax to obtain the optimized geometrics and the optimized separation between two slabs. The full relaxation of all models is quiet time-consuming but is precise and reliable.

3.3.1. Static Separations by UBER Method. Under UBER, the adhesion energy E_{ad} on the interslab separation d is defined as eq 1:[24]

$$E_{ad}(d) = -E_0(1 + (d - d_0)/s)\exp((d - d_0)/s) + C \quad (1)$$

Here E_0 is the ideal adhesive energy, d_0 is the equilibrium interfacial separation, s the scaling constant, and C is a constant to set the zero of the energy scale. The strength of the crystals measured by the maximum tensile stress perpendicular to the (0001) planes that can be withstood without spontaneous cleavage, shown in eq 2

$$\sigma_{max} = \frac{2E_0}{es} \quad (2)$$

where e is the base of the natural logarithm. This consequently yields the ideal adhesive energy (E_0), the equilibrium interfacial separation (d_0), and the ideal peak interfacial stress (σ_{max}). The fitted UBER curves for the four possible stacking configurations of 1-Ca-HA/Ti SI are shown in Figure 4a–d. Excellent fits are shown for all the cases indicating good validity of the UBER for metal–HA interfaces.

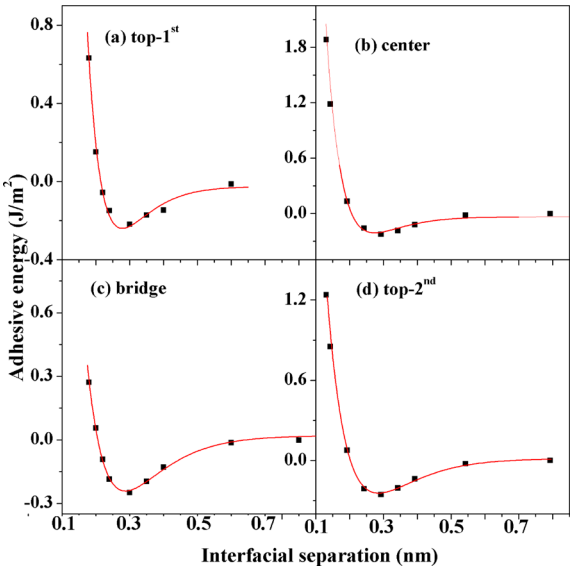

Figure 4. Adhesion energy as a function of the separation between the HA(0001) surface and Ti(0001) substrate for the Ca-terminated HA(0001)/Ti(0001) slabs with four stacking sites: top first (a), center (b), bridge (c), and (d) top second sites.

As shown in Figure 4, the bridge and top second have a slightly larger ideal adhesive energy (Figure 4c,d). The interfacial adhesion of the center is extremely weak as shown by the adhesive curve (Figure 4b), whereas the top first arrangement exhibits a modest ideal adhesive energy (Figure 4a). The adhesive curve of the top first arrangement results in a larger interfacial separation comparing to the bridge, the center, and the top second arrangements. These results are expected due to that the Ca atoms and Ti atoms are electropositive and repel each other. Table 2 listed details of the parameters in eqs 1 and 2 obtained by fitting the energy curves in Figure 4 for the quantitative comparison between the four interfacial models.

As shown in Table 2, the d_0 is slightly different for each of the considered configurations. The values of E_0 weakly depend on the stacking site of HA/Ti interface. The values of E_0 for center, top first, top second, and bridge sites interfaces are 0.17, 0.21, 0.258, and 0.26 J/m^2, respectively. It is noticeable that for the bridge-sited interfaces, the E_0 values are larger by 0.05, 0.09, and 0.002 J/m^2 compared to those of top first, center, and top second sites, respectively. Consequently, the bond between the HA and Ti will be stronger for the bridge-sited interfaces. However, the bridge-sited interface has much larger d_0 than the center-sited interfaces. For the case of bridge-sited interface, two of the interfacial Ti atoms locate at the bottom of the interfacial Ca atom, and therefore, the interfacial Ca atom and Ti atoms repel each other. The ideal peak of interfacial stress (σ_{max}) is 2.78, 2.0, 2.29, and 2.24 GPa for top first-, center-, bridge-, and top second-sited interfaces, respectively, which is in good agreement with the experimental value obtained by Forsgren et al.[43]

Table 2. Optimal Interslab Separations d_0 for Four Translational States of the 1-Ca-HA/Ti of SI Using UBER[a]

UBER	top 1st	center	bridge	top 2nd
d_0 (nm)	~0.278	~0.271	0.287	~0.285
E_0 (J/m^2)	~0.21	~0.17	~0.26	~0.258
σ_{max} (GPa)	~2.57	~2.0	2.29	2.24
s (nm)	0.0614	0.0638	0.084	0.0848

[a]UBER: the universal binding energy relation. SI: single interface.

3.3.2. Relaxed Separations. Second, dependences of total energies of fully relaxed 1-Ca-HA/Ti interface on the interfacial separations were checked. The interslab separation giving the lowest total energy of interface systems is selected as the optimum separation. It is reasonable to assume that this separation is valid for the other type of stacking, since only the stacking was differed in the considered interfaces. Two relaxation approaches, three Ti layers, and one HA layer of the slabs (denoted as HA/Ti-a), and all atoms (denoted as HA/Ti-b), were used to optimize the geometry of the supercell and the separation between the two slabs.

The relaxed separations together with total energies for the 1-Ca-HA/Ti interface are presented in Table 3. The optimum separations owning the lowest total energies are 0.227, 0.235, and 0.238 nm for HA/Ti-b, HA/Ti-a approaches of DI and SI, respectively. The minimum interfacial separations of them are 0.220, 0.235, and 0.235 nm, respectively. These are all slightly different from the Ti–Ti interlayer distance in bulk α-Ti ($P6_3/mmc$, 0.231 nm).[33] The equilibrium interfacial separation of the HA/Ti-b is slightly smaller than that of HA/Ti-a, due to the relaxation of atoms being far from the interface in the 1-Ca-HA/Ti-b slabs. However, the difference of the optimized interfacial separations obtained by the two methods is within 0.015 nm. For the PO_4-HA/Ti and 2-Ca-HA/Ti interfaces, the optimizations were performed by allowing top three Ti layers and one HA layer in the interfacial zone to relax, and the estimated interfacial separations are 0.248 and 0.369 nm, respectively.

For the d_0 and d_1 values of 1-Ca-HA/Ti shown in Tables 2 and 3, the fully relaxed method shows smaller minimum interfacial separations than those found by the UBER method. After optimization, the separation was enlarged for HA/Ti-a relaxation method when the initial separation was in the range 0.153–0.248 nm. Otherwise, the separations (except for the 0.302 nm) were all increased after relaxation by the HA/Ti-b method. The discrepancy on the separation by the two methods may originate from the fact that there is about a 6.2% misfit along the interface between HA(0001) and

Table 3. Initial Separation d_i and Optimized Separation d_1 between Two Slabs for the 1-Ca-HA/Ti Using Different Relaxation Methods[a]

	HA/Ti-a double-interfaces			HA/Ti-b double-interfaces	
original d_i (nm)	relaxed d_1 (nm)	E_{tot} (eV)	single-interface E_{tot} (eV)	relaxed d_1 (nm)	E_{tot} (eV)
0.153	0.235	−1015.938	−1013.170	0.220	−1021.583
0.165	0.238	−1015.613	−1013.512	0.227	−1023.166
0.215	0.245	−1014.888	−1012.714	0.253	−1022.636
0.231	0.238	−1015.582	−1013.486		
0.248	0.261	−1014.089		0.277	−1021.451
0.265	0.242	−1014.627	−1013.339	0.285	−1020.530
0.283	0.257	−1015.064		0.288	−1019.099
0.302				0.288	−1018.881
0.315	0.339	−1012.946	−1011.178	0.331	−1020.314
0.365	0.426	−1011.296	−1009.826	0.408	−1016.578
0.415	0.483	−1010.835	−1009.459	0.454	−1015.634
0.55	0.616	−1008.844	−1009.329	0.611	−1014.612
0.7	0.770	−1008.591	−1009.279	0.765	−1014.517

[a] d_1 is defined as the average separation between the first Ti layer nine atoms and the seven nearest atoms of HA. In HA/Ti-a and HA/Ti-b, a and b denoted all atoms relaxed and partial atoms relaxed approaches.

Ti(0001) surfaces, which causes the rotation of PO_4, and an inward movement of Ca atom at the interface by the relaxation, whereas the UBER method does not account these effects. Therefore, the full relaxation results are treated as the equilibrium values for the four cases studies here.

3.3.3. Optimized Interface Structures. The interface structures with the optimum interslab separations after relaxation are presented in Figures 5 and 6. The typical pattern of HA/Ti interfaces was the formation of different Ti−O bonds

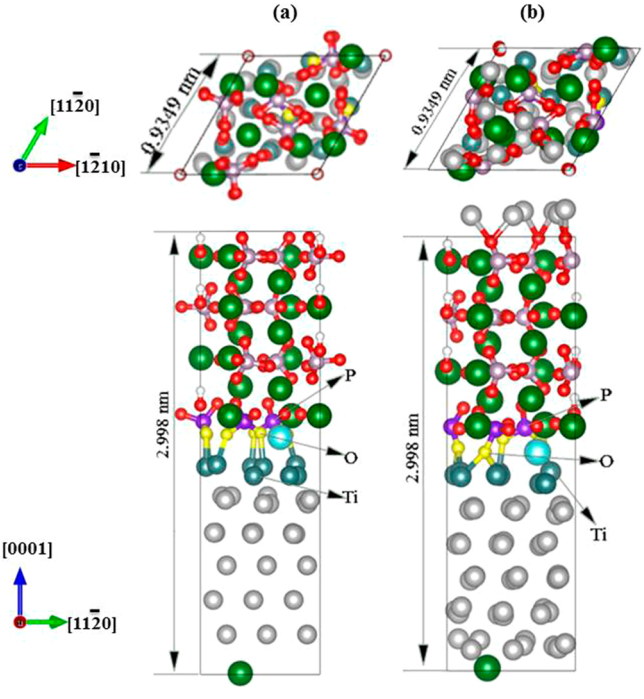

Figure 5. Top and side views of slab models of the 1-Ca-HA/Ti double interfaces after (a) three Ti layers and one HA layer relaxation and (b) all atoms relaxation.

between the Ti slab and PO_4 groups in HA at the interface. Several interesting features in the optimized interface structures can be seen. (1) For 1-Ca-HA/Ti cases, six Ti−O bonding species with the length 0.20−0.24 nm across the interface were generated, and there is no distinct difference in the interface structure between the DI and SI models. (2) Strong distortion on atomic positions occurred in the Ti side during the optimization, while the atomic coordinates in the HA side are almost kept unchanged regardless the terminations of the HA surface. (3) The bottom Ti layers show a zigzag structure after all atoms relaxation. (4) Both structures possess not very good coordination and therefore weak bonding. (5) Metal-to-metal stacked 2-Ca-HA/Ti demonstrates a repulsion of Ca atoms from the Ti slabs, enlarging the separation between the two subslabs.

The structural information on the considered HA/Ti interfaces is presented in Table 4. The interfacial separation after relaxation is the average of separations between the nine Ti atoms of Ti slab and six O atoms and one Ca atom of HA at the interface, since the z coordinate values of atoms at the interface perpendicular to the (0001) surface are quite different after relaxation. This is particularly true for the interfacial Ti layer (layer 1) shown as blue-green balls in Figures 5 and 6. The layers have been designated according to their distances from the interface; e.g., layer 1 is closer to the interface region than layer 2 and so forth. Change of the interlayer spacing Δd_{ij} is defined as a percentage of the spacing in the bulk $\Delta d_{ij} = ((d_{ij} - d_{ij}^0)/d_{ij}^0)$, where d_{ij} denotes the distance between the ith and jth atomic layers, and d_{ij}^0 is the value before structural optimization. The optimization geometries of DI are shown in Figure 5, 1-Ca-HA/Ti-a (Figure 5a) and 1-Ca-HA/Ti-b (Figure 5b), and SIs are shown in Figure 6, 1-Ca-HA/Ti-a (Figure 6a) and 1-Ca-HA/Ti-b (Figure 6b), PO_4-HA/Ti-a (Figure 6c), and 2-Ca-HA/Ti-a (Figure 6d).

Since 1-Ca-HA/Ti and PO_4-HA/Ti are the most promising interface structures, we analyze their geometries in more detail. In 1-Ca-HA/Ti, there are four to six Ti−O bonds across the interface, and the shortest Ti−O bond length is around 0.20 nm, close to the experimental Ti−O bond length in the bulk TiO_2 ($I4\bar{1}/amd$, 0.198 nm),[44] indicating a strong Ti−O bonding between the HA/Ti interface. The formation of the strong Ti−O bonds has large effects on geometric structures of the HA layers and Ti layers. For example, as shown in Table 4, the distance between the nearest interface PO_4 layer and the second nearest interface PO_4 layer along the [0001] direction are greatly enlarged by 19.8% as compared with that of bulk HA. The deviations of the respective (0001) interlayer distances from the interface PO_4 layer to the central of PO_4 layer are 19.8% and 8.7%. The total size of the HA(0001) slab is expanded by 6.4% along the [0001] direction. On the contrary, the interlayer distances of the six Ti(0001) atomic layers of the supercell are shrunk, and the deviations of the respective (0001) interlayer distances from the interface Ti layer to the central Ti layer are −10.7%, −2.9%, and 6.0%.

For PO_4-HA/Ti interface, four Ti−O bonds with the length about 0.20 nm are formed across the interface, which is the smallest distance in Table 4. The shorter Ti−O bond length is consistent with the larger adhesive energy of the HA/Ti interface compared with the other two termination interfaces. For the PO_4-terminated interface, the interlayer distance is enlarged by 10.1% for the interface PO_4 layer and 6.1% for the subinterface PO_4 layer, respectively. The deviations of the

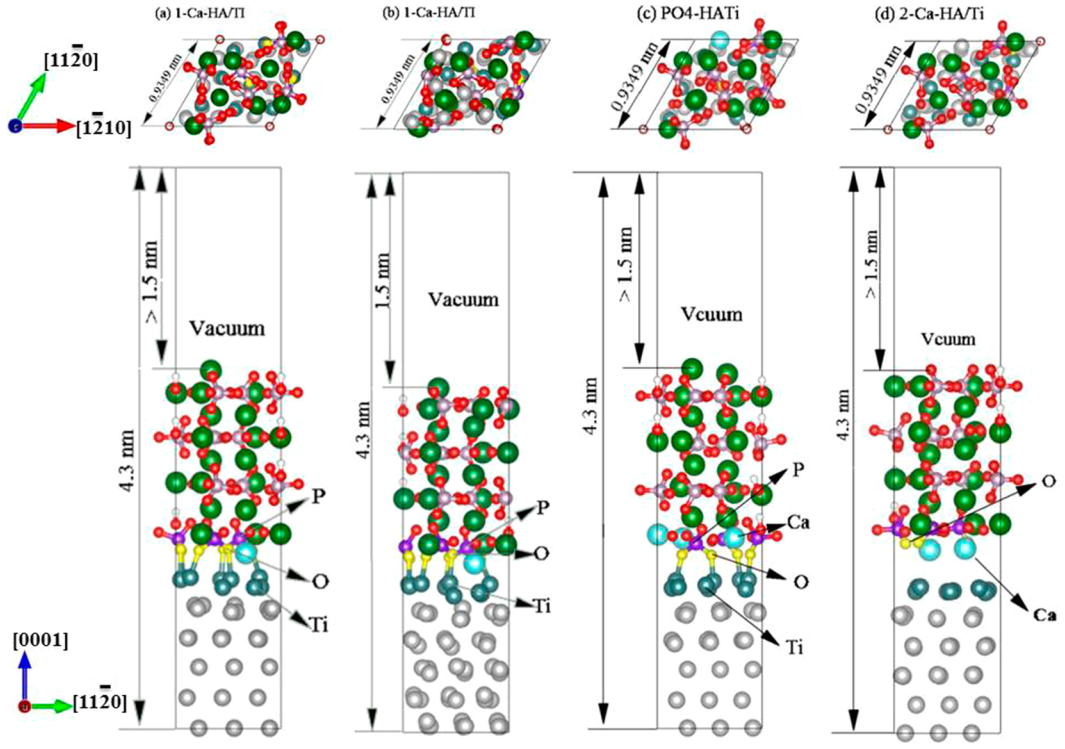

Figure 6. Top and side views of single interface models of the 1-Ca-HA/Ti: (a) by three Ti layers and one HA layer relaxing and (b) by all atoms relaxing, and of (c) PO_4-HA/Ti and (d) 2-Ca-HA/Ti interfaces with relaxation same as in part a.

Table 4. HA(0001)/Ti(0001) Interface Relaxation Dependence on Relaxation Methods and the HA to Ti Interfacial Separations[a]

		HA/Ti-a				HA/Ti-b 1-Ca-			
			1-Ca-						
	interlayer	PO_4-SI	SI	DI	2-Ca-SI	SI		DI	
original d_i (nm)		0.24	0.231	0.259	0.24	0.165	0.215	0.209	0.359
relaxed d_1 (nm)		0.248	0.238	0.245	0.369	0.230	0.228	0.227	0.331
nm	Δ	0.08	0.07	−0.14	0.13	0.75	0.13	0.28	−0.51
Ti	Δd_{12}	−9.7%	−10.7%	−9.4%	−11.8%	−13.9%	−10.7%	−11.3%	−8.7%
	Δd_{23}	−6.2%	−2.9%	−6.4%	−5.1%	−7.2%	−6.2%	−6.5%	−4.3%
	Δd_{34}	−7.6%	−6.0%	−8.0%	−6.1%	−9.6%	−7.0%	−5.2%	−6.7%
	Δd_{45}					−7.0%	−5.1%	−5.2%	−5.0%
	Δd_{56}					−13.1%	9.2%	−12.1%	−6.8%
P	Δd_{12}	10.1%	19.8%	7.6%	0.01%	9.1%	5.0%	6.3%	19.4%
	Δd_{23}	6.1%	8.7%	1.1%	9.1%	1.4%	1.7%	2.1%	5.8%
	Δd_{34}					7.0%	7.5%	7.6%	7.7%
Ti−O dist (nm)		0.20−0.207	0.217−0.235	0.206−0.215	0.23	0.208−0.234	0.209−0.228	0.211−0.230	0.208−0.220
no. Ti−O		4	6	4	1	6	6	5	5

[a]Change of the interlayer spacing Δd_{ij} as a percentage of the spacing in the bulk $\Delta d_{ij} = ((d_{ij} - d_{ij}^0)/d_{ij}) \times 100\%$. SI: single interface in the model. DI: double interface in the model. PO_4-, 1-Ca-, and 2-Ca- mean PO_4-terminated, 1-Ca-terminated, and 2-Ca-terminated; HA-a and HA-b denote partial and all atoms relaxations in the interfacial supercell.

Ti(0001) interlayer distances from interface Ti layer to the central Ti layer are −9.7%, −6.2%, and −7.6%.

For 2-Ca-HA/Ti interface, there is only one pair of Ti−O atoms with the distance shorter than 0.24 nm, which is the weakest interfacial interaction in Table 4 and consistent with the smallest adhesive energy as mentioned above. Upon relaxation, absolute deviations for interlayer distances are less than 1% for interfacial PO_4 layers.

Overall, the HA(0001) side shows the rotation of PO_4 and a inward movement of Ca atoms at the interface with expanding along the *c* direction and the Ti(0001) side shows a rippled relaxation with reduced interlayer spaces, respectively. Due to the lattice misfit and the formation of the Ti−O interfacial bonds across the interface, the HA(0001) side expands in the *c* direction, with shrinkages in the (0001) surface, and the variation in the Ti(0001) side is in an opposite way.

dx.doi.org/10.1021/am504734d | ACS Appl. Mater. Interfaces 2014, 6, 20738−20751

Table 5. Work of Adhesion W_{ad} and the Interface Energy γ_{int} versus the Interfacial Separation d_i and d_1 for 1-Ca-HA/Ti Interface Models

	HA/Ti-a				HA/Ti-b	
	double-interfaces		single-interface		double-interfaces	
original d_i (nm)	relaxed d_1 (nm)	W_{ad} (J/m^2)	W_{ad} (J/m^2)	γ_{int} (J/m^2)	relaxed d_1 (nm)	W_{ad} (J/m^2)
0.153	0.235	−1.14	−1.40	3.11	0.220	−1.99
0.165	0.238	−1.10	−1.52	3.07	0.227	−1.92
0.215	0.245	−0.95	−1.47	3.16	0.253	−1.63
0.231	0.238	−0.95	−1.47	3.07		
0.248	0.261	−0.94			0.277	−1.74
0.265	0.242	−0.95	−1.27	3.09	0.285	−1.47
0.283	0.257	−0.79			0.288	−1.64
0.302					0.288	−0.95
0.315	0.339	−0.70	−0.36	3.32	0.331	−1.35
0.365	0.426	−0.28	−0.22	3.46	0.408	−0.20
0.415	0.483	−0.22	−0.13	3.50	0.454	−0.05
0.55	0.616	−0.04	−0.09	3.51	0.611	−0.01
0.7	0.770	−0.01	−0.01	3.52	0.765	−0.003

3.4. Work of Adhesion. The work of adhesion is used to measure the bonding strength at the interface. Following the method proposed by Finnis and his colleague,[45] the work of adhesion can be used to evaluate the interface energy at finite temperature.[44] The work of adhesion between the HA(0001) surface and the Ti(0001) surface was calculated by using the following definition (eq 3):

$$W_{ad} = [E_{HA/Ti} - E_{HA(0001)} - E_{Ti(0001)}]/NA \quad (3)$$

Here $E_{HA/Ti}$ is the total energy of the interface system in its optimized geometry, $E_{HA(0001)}$ and $E_{Ti(0001)}$ are the total energies for the corresponding isolated subsystems with the same geometry as that of the optimized interface system, and A represents the interface area. The factor N accounts for the presence of one interface (N = 1 or 2 for the HA/Ti single interface model or two interfaces for the HA/Ti double interface model).

The work of adhesion calculated by eq 3 versus the interfacial separations is presented in Table 5. The value of obtained W_{ad} is more negative with the decreasing interslab separations and is close to zero when the separation is larger than 0.55 nm for all the considered supercells. The absolute value of W_{ad} obtained the maximum of about 0.24 or 0.22 nm interslab separation for HA/Ti-a and HA/Ti-b, respectively. The original separation shorter than 0.153 nm is not listed in Table 5. The relaxed interfacial models are not reasonable, and their total energies cannot converge within 0.01 eV/unit when the original interslab separation is smaller than 0.15 nm. In a comparison of the corresponding values of W_{ad}, it can be seen that the HA/Ti-b possesses the larger interfacial adhesion (W_{ad} = −1.99 J/m^2) than HA/Ti-a, indicating that the all atoms relaxed interface is readier to form stronger bonds at the interface.[46,47] However, the large number of atoms in the interfacial supercell makes the calculation of all atom relaxation extremely time-consuming. Therefore, the method of partially relaxed atoms near the interface is a good approach. There are no experimental or theoretical results about the HA/Ti interface. However, similar values of the work of adhesion were obtained for Mg(0002)/Al_2CO(0001),[47] Fe_4N/MoS_2,[48] Pt-HfO_2,[49] and $LiFePO_4/FePO_4$ interface systems.[50] However, double-interface or single-interface has influence on the adhesion properties of the HA/Ti interface. For example, the most negative W_{ad} is −1.14 J/m^2 and the smallest d_1 is 0.235 nm for the optimal interface structure of double-interface interfaces while those of the single-interface interfaces are 1.52 J/m^2 and 0.238 nm, respectively. The single-interface model is more suitable for investigation of the interfacial adhesion strength and is therefore used to analyze the electronic structures of HA/Ti interfaces in the next section.

Table 6 presents the calculated work of adhesion W_{ad} of the three considered sequences after geometric optimization with the optimizing interfacial separations between HA(0001) and Ti(0001) interfaces. As shown in Table 6, for 1-Ca-HA/Ti interface, DI or SI in slab models and partial or full relaxed both have influence on the value of adhesion work. Thus, the W_{ad} was calculated on the SI interface models by relaxing atoms near interface for 2-Ca-HA/Ti and 1-Ca-HA/Ti interfacial slabs.

Table 6. Calculated Work of Adhesion [W_{ad} (in J/m^2)] and the Interface Energy (γ_{int}) of Ti(0001) on HA(0001) with PO_4-Rich, Ca-Rich, and Stoichimetric-Terminated HA(0001)

system	W_{ad} (J/m^2)	$\gamma_{int}t$ (J/m^2)
PO_4-HA/Ti-a	−2.33	3.48
2-Ca-HA/Ti-a	−0.80	3.73
1-Ca-HA/Ti-a DI	−1.10	2.85
1-Ca-HA/Ti-b DI	−1.92	2.05
1-Ca-HA/Ti-a SI	−1.52	3.07

From Table 6, it is obvious that PO_4-HA/Ti gives stronger affinity than 2-Ca-HA/Ti and 1-Ca-HA/Ti. The stronger Ti−O bonding across the interface is mainly due to the more reactive nature of the PO_4-termination surface. The work of adhesion of metal-to-metal stacking 2-Ca-HA/Ti is smallest but still negative. The one Ca atom terminated interface, 1-Ca-HA/Ti, reveals relatively weak bonding, though much stronger than the interface with two Ca atoms' termination. For PO_4-HA/Ti and 1-Ca-HA/Ti interfaces, the bottom oxygen layer comprises six O atoms, which may attract electrons from Ti to compensate the charge deficiency. On the contrary, for 2-Ca-HA/Ti, two Ca atoms may transfer out electrons to Ti to stabilize the surface.

dx.doi.org/10.1021/am504734d | ACS Appl. Mater. Interfaces 2014, 6, 20738−20751

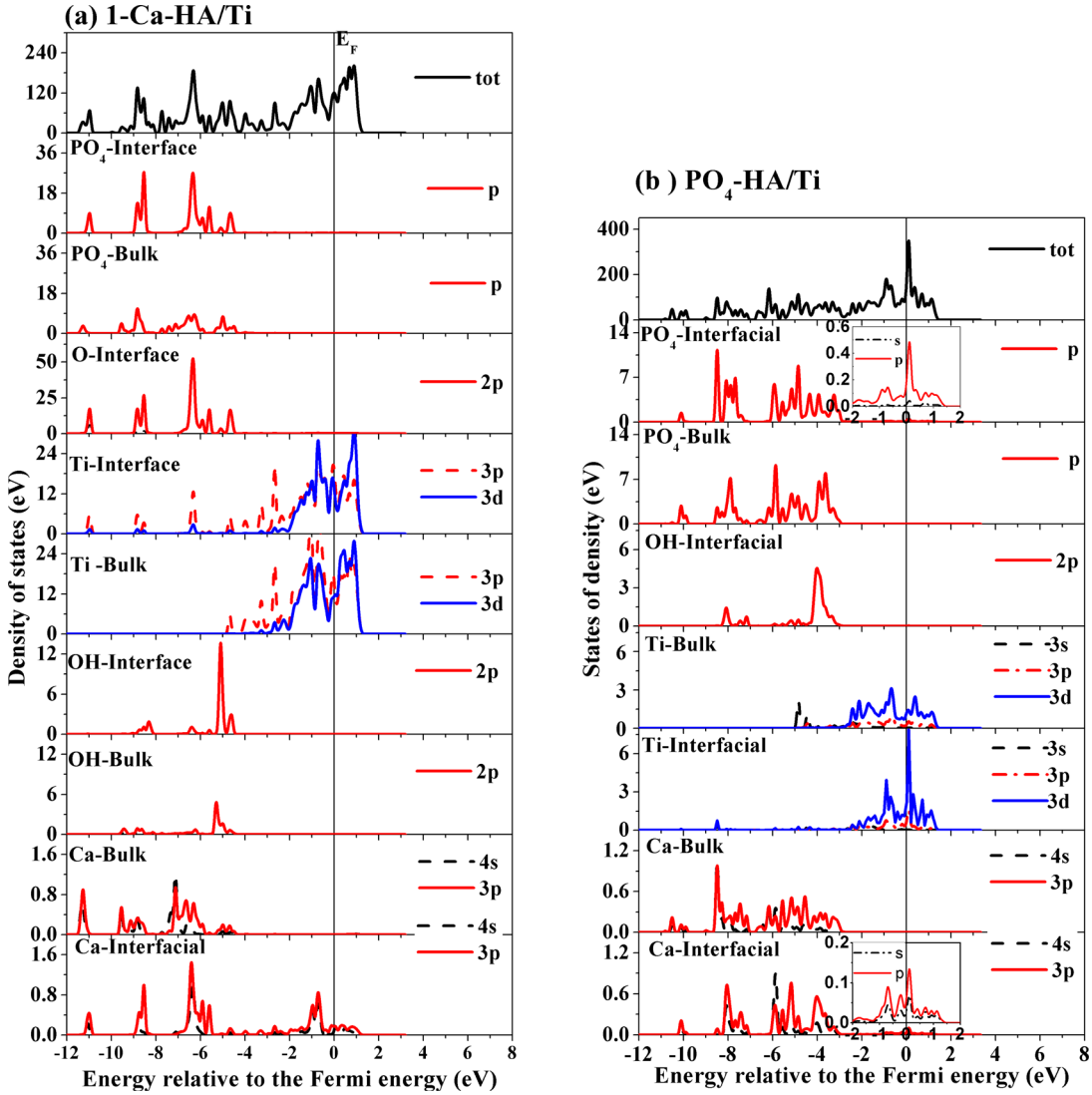

Figure 7. Total and partial DOSs of (a) 1-Ca-HA/Ti and (b) PO_4-HA/Ti interfaces. The insets in part b are the partial DOSs of interfacial PO_4 group and Ca atom distributed in (−2 to 2) eV energy range in the second and bottom panels, respectively.

3.5. Interface Energy. Another thermodynamic quantity usually associated with interface thermodynamic stability is the interface energy γ_{int}, which originates from the change in the interfacial bonding and the structure strain and can be defined as the excess energy per unit area of a system due to the forming interface. The interfacial energy for the single-interface model is evaluated via the following definition

$$\gamma_{int} = [E_{HA/Ti} - N_{HA}E_{HA} - N_{Ti}E_{Ti}]/A \quad (4)$$

where E_{HA} and E_{Ti} are the total energy of the per formula bulk HA and the unit cell of the bulk α-Ti, respectively.

The calculated γ_{int} is also listed in Table 5, which is obtained for interfacial supercells with the lowest total energy. Same as interfaces consisting of dissimilar compounds, HA/Ti interfaces are composed of phases with different structures and chemical bonds. Therefore, the energy difference between the interface and the single bulk phases can be expected to be relatively high. For the HA(0001)/Ti(0001) interface, the absolute values of the interfacial energies are larger than the surface energies of the HA(0001) and the Ti(0001) as well as the works of adhesion. One of the reasons for this result can be attributed to the high elastic energy of the (0001) interface induced by lattice mismatch. Indeed, the elastic energy is incremented after being fully relaxed and the HA(0001) side is stretched while the Ti(0001) side is compressed perpendicular to the (0001) plane. The positive value of γ_{int} is implying that the formation of a new phase due to the interfacial atoms diffusion is not likely to happen at the HA(0001)/Ti(0001) interface.

3.6. Electronic Structure and Bonding. To further understand the interaction between HA and Ti, we have calculated total and partial densities of states (DOS) for each interface model. As examples, most stable configurations, 1-Ca-HA/Ti and PO_4-HA/Ti, the electronic structures in terms of DOS are analyzed (see Figure 7a,b). Previously, we reported that the total DOS of HA shows a 5.7 eV band gap between the valence and conduction bands, and four bonding areas in the valence band which are mainly contributed by PO_4 unit.[35] On the contrary, the total DOS of the HA/Ti interface shows a metallic characteristic in both the Ca atom and PO_4-terminated interfaces. The PDOSs indicate that the metallic nature mainly comes from Ti. Several important features can be seen from the total and partial DOSs in Figure 7a. First, Figure 7 a shows an interaction between O 2p and Ti 3d electrons in the valence band at around −4.6 and 6.4 eV, which are the main ionic

dx.doi.org/10.1021/am504734d | ACS Appl. Mater. Interfaces 2014, 6, 20738−20751

components of bonding across the interface. Similarly, mixing of Ti d and Ca s,p states can also be observed near the Fermi energy in this figure. Second, the PDOSs of the interfacial Ti atoms in the 1-Ca-HA/Ti slab show new peaks in the energy range from −8.8 to −4.0 eV, and they overlap with the O p orbitals at the same energy level in the HA(0001) slab. These overlapping states contribute to the hybridization of Ti and O orbitals, which confirms clearly the existence of Ti−O bonds in the HA(0001)/Ti(0001) interface. Third, the partial DOSs of the interface atoms also show a finite state at the Fermi level, indicating metallic bonding across the interface, arising mainly by the Ti d and Ca s, p states. Finally, the appearance of sharp peak of Ti 3 d states at the Fermi energy is found in the PDOS of Ti layer situated right at the interface. The DOS for the interfacial OH unit shows a weak interaction between O 2 p and Ti 3 d electrons in the valence band at around −4.6 and 6.4 eV. Taking into account the higher coordination of Ti and O compared to Ca, it may conclude that Ti−O interaction contributes strongly to the interfacial bonding. Comparing the PDOSs of the same elements (or groups) in an interface which are in bulk layers (Figure 7a), one can find that the valence charge accumulation and depletion are more obvious in the central interfacial layer than in both side layers. For example, the valence electron transfers of the Ti-interface layer are much greater than those in the Ti-bulk layers, and Ca atoms have the same consequence too. That indicates that the interfacial bonding mainly depends on the interaction of the first interfacial layers of Ti(0001) and HA(0001) slabs. The DOS of the interfacial Ti atoms shows that there is a large amount of depleted state in the energy range from −6.0 to 2.0 eV. On the contrary, the DOS of the interfacial PO_4 and OH groups shows that there are valence charge accumulations from −9 to −4.4 eV. The charge transfers mainly are contributed by the interfacial Ti 4s, and its DOS is less localized than the interior bulk layer. Therefore, the interfacial electron interaction strengthens the metallic characteristics of Ti atoms, and the ionic Ti−O bonds are likely formed across the PO_4-terminated interface. The DOSs of interfacial Ca atoms are obviously less localized than the interior bulk layer, and the metallic characteristics are strengthened.

The mechanism of the chemical bond at the HA(0001)/Ti(0001) interface was visually demonstrated by the distributions of the total charge density of valence electrons, as well as the difference charge density defined as

$$\Delta\rho(r) = \rho_{\mathrm{HA/Ti}}(r) - \rho_{\mathrm{HA(0001)}}(r) - \rho_{\mathrm{Ti(0001)}}(r) \quad (5)$$

where $\rho_{\mathrm{HA/Ti}}(r)$ is the electron density of the total HA(0001)/Ti(0001) interface system, and $\rho_{\mathrm{HA(0001)}}(r)$ and $\rho_{\mathrm{Ti(0001)}}(r)$ are the unperturbed electron densities of the isolated HA(0001) and Ti(0001) slabs, respectively. The charge distributions and atomic structures projected on $(01\bar{1}0)$ are shown in Figure 9a, and charge different distributions (CDD) projected on $(1\bar{1}00)$ of this system are illustrated in Figure 9b. From Figure 9a, it can be found that the charge distributions of O atoms are more localized and positive than those of Ti atoms. The more negative the blue mark is in the figure, the more electrons the atoms lose. As shown in Figure 9b, the electron charge rearrangements are mainly confined to two atomic layers near the interface. Thus, the O and Ti sites, are intermediate to build the interface, and possess different charge density difference. An ionic bond between O and Ti atoms across the interface was detected. Ti atom acts as an electron donor in this system as negative CDD was found in its vicinity.

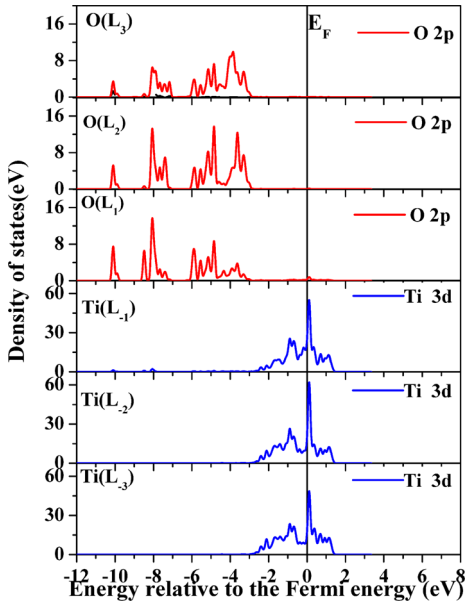

Figure 8. Local density of states of the PO_4-HA/Ti interface. Each panel corresponds to one kind of atoms in a specific layer specified as L_i, where the index i counts the layers from the interface and positive or negative indicates HA side or Ti side, respectively.

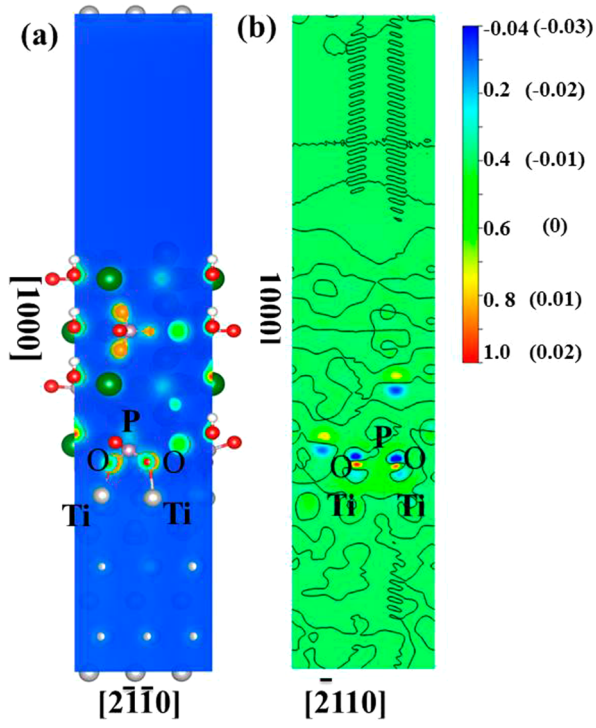

Figure 9. Charge distribution with atomic structure and CDD projected on the $(1\bar{1}00)$ plane of the 1-Ca-HA/Ti interface.

The DOSs of PO_4-HA/Ti are shown in Figure 7b, in which the partial DOS of interfacial PO_4 units and the Ca atom in the energy range −2 to 2 eV are highlighted in the insets. The partial DOSs of the interfacial PO_4 unit, Ti atoms, and Ca atoms were changed compared to the 1-Ca-HA/Ti interface. A strong interaction between PO_4 unit and Ti atoms was detected owing to the increase of overlaps between the two groups near

dx.doi.org/10.1021/am504734d | ACS Appl. Mater. Interfaces 2014, 6, 20738−20751

the Fermi energy level, as shown in the insets of partial DOSs of the interfacial PO_4 group. The partial DOSs of the PO_4 unit and Ti atoms also show a finite DOS at the Fermi energy, indicating metallic bonding across the interface, arising mainly because of Ti d and PO_4 p states. The DOS from Ca p states at the Fermi level is almost negligible, suggesting non-Ti−Ca intermetallic bonding at the interface. It is worth noting that a larger amount of PO_4 p states appears in the energy range from −8.6 to −7.5 eV, while the partial DOS of the interfacial Ti atoms shows a larger amount of depleted state at that energy region. Thus, charge transfer from Ti 4s to O atom occurs, and the interaction between Ti and O atoms is enhanced. This may be the reason that the work of adhesion of PO_4-HA/Ti is more negative than that of the Ca terminated HA/Ti interfaces as shown in Table 6.

As an example, the local density of states (LDOS) for the PO_4-HA/Ti slab is shown in Figure 8. The LDOS reflects the changes of the bonding across the interface. The appearance of the peak at around −0.2 eV of Ti 3 d state of Ti layer at the interface [Ti(L_{-1})] indicates the presence of a localized interface state. The sharp peak around the Fermi energy level of the sub-Ti layer below the interface [Ti(L_{-2})] shows larger amplitude than that of the Ti layer further away the interface [Ti(L_{-3})], which may cause the lesser stability of Ti(L_{-2}) compared to that of the Ti(L_{-3}). The O 2p peaks in the PO_4 group at −3 to −5 eV were decayed at the interface while the amplitudes of the O 2p peaks in PO_4 group at −10 and −8 eV were magnified at the interface. The sharp peak at −8 eV is very pronounced in the O layer of PO_4 group and overlaps the peak of Ti 3d appearing in the LDOS of the Ti layer at the interface. Finally, the appearance of not so large peaks at the Fermi energy is found in the LDOS of the O layer situated the interface.

The atomic structure, charge distribution, and CDD on the $(10\bar{1}0)$ surface of this system are shown in Figure 10a,b. Clearly, the covalent bonding between P and O atoms within the PO_4 unit is illustrated, and the ionic bonding between O and Ti atoms at the interface is also detectable.

In summary, for the HA(000)/Ti(0001) interface, the PO_4-HA/Ti has more preferable stacking and is more stable in thermodynamics than the Ca-terminated interfaces. The dominant bonds are the ionic interactions between interfacial atoms, especially the Ti−O bonds.

The plane-averaged charge (PAC) is shown in Figure 11. The PAC shows the spatial distribution and rearrangement of electronic charge along the specified direction. The direction that is perpendicular to the interface plane (c) is selected to study the charge transfer across the interface. The PACs show an insight into the charge transfer near the interface. A perturbation of the density distribution near the interface is clearly shown caused by the free surface of each slab.

The PAC of the relaxed PO_4-HA/Ti supercell is illustrated in Figure 11a. The electronic density across the interface is greatly inhomogeneous in the HA slab compared to the titanium slab. The second characteristic is a fairly great charge rearrangement in a near-interface region about 0.5 nm thickness (Δ curve in Figure 11a).

Figure 11b provides the PAC of the relaxed 1-Ca-HA/Ti interface. The charge distributions of the Ti side in this case are quite similar to that of the PO_4-HA/Ti. The charges accumulate in the subinterface layer of the HA side between the titanium layer from Ti side and the third interface layer from the HA side. The PAC difference is smaller compared to

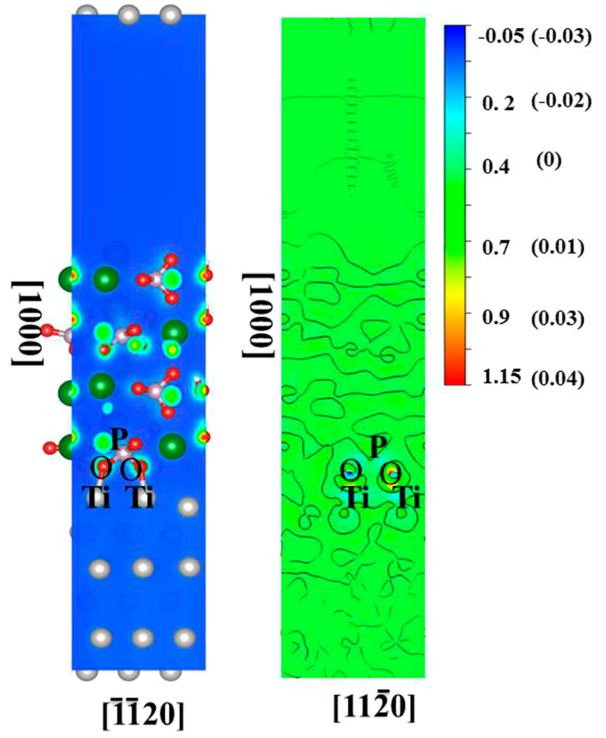

Figure 10. Atomic structure, charge distribution, and CDD projected on the $(10\bar{1}0)$ plane of the PO_4-HA/Ti interface.

PO_4-HA/Ti; however, the region is affected by the interface is also about 0.5 nm thickness.

Far from the interface, the spatial charge distribution in the stacked 2-Ca-HA/Ti (see Figure 11c) interface is quite similar to that of the PO_4-HA/Ti. The charge distribution in the vicinity of interface can seem as the superposition of charge distribution of the individual slabs. Due to the weak bonding at the interface, the charge rearrangement at the interface is much smaller, and appears mostly in the ∼0.5 nm thick region around the interface.

To summarize, the PACs of considered structures show a rearrangement of charge depending on stacking. The alteration of the electronic density mainly happens in a ∼0.5 nm thick region in the interface. The bonding strength at the interface measured by the work of adhesion can be correlated with the amplitude of the difference in PACs.

This correlation becomes more obvious, after the work of adhesion was plotted as the integral charge transfer (see Figure 12). The latter is obtained by the integration over the absolute value of Bader difference of the supercell and could be treated as an indirect measure of the local charge transfer. It is clear that the two Ca atoms' terminated 2-Ca-HA/Ti interface shows rather small charge transfer, and its work of adhesion is below 1.0 J/m^2. The PO_4-HA/Ti and 1-Ca-HA/Ti systems exhibit a slightly larger charge transfer, and their works of adhesion are −2.33 and −1.52 J/m^2, respectively.

4. CONCLUSION

The first-principles density functional calculations were performed to study the affinity properties of the HA(0001)/Ti(0001) interface with a lattice mismatch of 6.2%. Three different stacks and two interface models have been considered. Two methods, the full relaxation and the UBER, were applied to determine the interfacial separation and

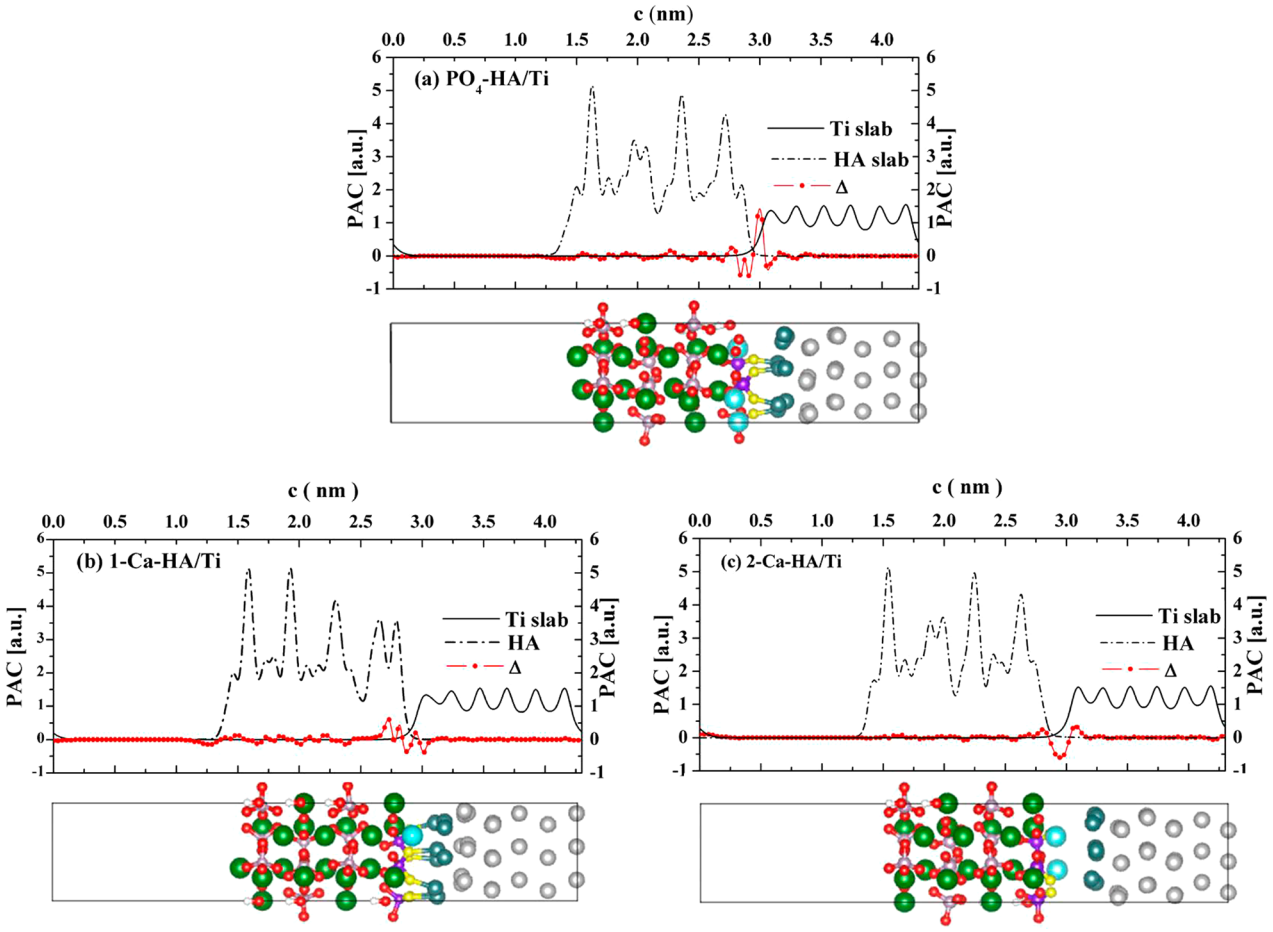

Figure 11. Plane-averaged charge (PAC) of the relaxed structures. Δ stands for the difference between the PACs of the superlattice and the sum of PACs of the individual HA(0001) and Ti(0001) slabs.

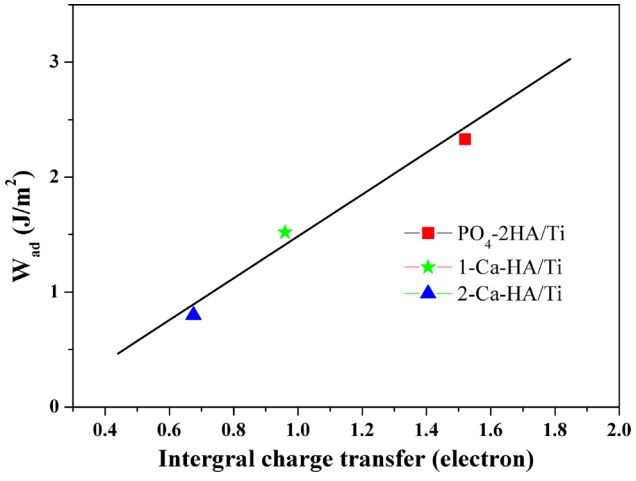

Figure 12. Dependence of work of adhesion on integral charge transfer.

the atomic arrangement in the interfacial zone. After relaxation, the minimum interfacial separation is 0.235 nm (0.220 nm) obtained by HA/Ti-a (HA/Ti-b) approaches for the 1-Ca-HA/Ti interface, 0.248 nm for PO_4-HA/Ti interfaces, and 0.369 nm 2-Ca-HA/Ti interfaces, respectively. On the basis of the calculations, the most stable interface models (1-Ca-HA/Ti and PO_4-HA/Ti) have been identified. It was found that the typical pattern of HA/Ti interfaces was the formation of different Ti−O bonds across the interface. A maximum of six Ti−O bonds with the lengths of 0.20−0.24 nm for the 1-Ca-HA/Ti interface and four Ti−O bonds with lengths around 0.20 nm for the PO_4-HA/Ti interface result in the strong adhesion: W_{ad} = −1.52 J/m^2 for the former and −2.33 J/m^2 for the latter. On the contrary, the metal-to-metal stacking (2-Ca-HA/Ti) gives the weakest adhesion (W_{ad} = −0.80 J/m^2). The geometry optimizations of interface models by partial and all atoms relaxations influence the work of adhesion. The all atoms relaxation possesses the stronger interfacial adhesion (−1.99 J/m^2) than the partial atoms relaxation (−1.14 J/m^2) for DI of 1-Ca-HA/Ti. The evaluated adhesion properties of the HA/Ti interface also depend on the interface model, DI or SI. For example, the most negative W_{ad} is −1.14 J/m^2, and the smallest d_0 is 0.235 nm for the optimal 1-Ca-HA/Ti interface structure of DI, while those of the SI interfaces are −1.52 J/m^2 and 0.235 nm, respectively. Analysis of the electronic structure has shown that the existence of undercoordinated atoms at the interface leads to a variety of features in the DOSs, ranging from metallic characteristic in both the Ca- and PO_4-terminated interfaces to overlapping states of O 2 p and Ti 3 d electrons (Ti−O across the interface). It has been found that the charge rearrangement in the interface is a key factor determining the work of adhesion; i.e., those interfaces that show high charge rearrangement also have a strong adhesion and vice versa.

dx.doi.org/10.1021/am504734d | ACS Appl. Mater. Interfaces 2014, 6, 20738−20751

■ ASSOCIATED CONTENT

Supporting Information

Models of HA and Ti low index surfaces, convergence tests of surface energy with respect to slab thickness and relaxation method, and the atomic structures of different atom terminations. 1-Ca, 2-Ca, and PO_4-1 of HA(0001) surfaces after relaxation, Figure S2. The $(01\bar{1}0)$, the $(10\bar{1}1)$, the $(11\bar{2}0)$, and the $(01\bar{1}1)$ of HA surfaces models and their surface energies, Figure S3 and Table S1, respectively. This material is available free of charge via the Internet at http://pubs.acs.org/.

■ AUTHOR INFORMATION

Corresponding Author

*E-mail: sy@hitwh.edu.cn. Phone: +86-631-5687772.

Notes

The authors declare no competing financial interest.

■ ACKNOWLEDGMENTS

This work was supported by the National Basic Research Programme of China, Grant 2011CB606400-G, the Natural Science Foundation of Shandong, China, Grant ZR2010BM034.

■ REFERENCES

(1) Ripamonti, U.; Roden, L. C.; Renton, L. F. Osteoinductive Hydroxyapatite-Coated Titanium Implants. *Biomaterials* **2012**, *33*, 3813−3823.

(2) Baker, M. A.; Assis, S. L.; Higa, O. Z.; Costa, I. Nanocomposite Hydroxyapatite Formation on a Ti-13Nb-13Zr Alloy Exposed in a MEM Cell Culture Medium and the Effect of H_2O_2 Addition. *Acta Biomater.* **2009**, *5*, 63−75.

(3) Elliott, J. C. Structure and Chemistry of the Apatites and Other Calcium Orthophosphates. In *Studies in Inorganic Chemistry*; Elsevier: Amsterdam, 1994.

(4) Kim, S. Y.; Kim, D. H.; Kim, Y. G.; Oh, C. W.; Ihn, J. C. Early Failure of Hemispheric Hydroxyapatite-Coated Acetabular Cups. *Clin. Orthop. Relat. Res.* **2006**, *446*, 233−238.

(5) Nguyen, H. Q.; Deporter, D. A.; Pillar, R. M.; Valiquette, N.; Yakubovich, R. The Effect of Sol-Gel-Formed Calcium Phosphate Coatings on Bone Ingrowth and Osteoconductivity of Porous-Surfaced Ti Alloy Implants. *Biomaterials* **2004**, *25*, 865−876.

(6) Wei, X.; Fu, C.; Savino, K.; Yates, M. Z. Fully Dense Yttrium-Substituted Hydroxyapatite Coatings with Aligned Crystal Domains. *Cryst. Growth Des.* **2012**, *12*, 217−223.

(7) Garciasanz, F. J.; Mayor, M. B.; Aris, J. L.; Pou, J.; León, B.; Peŕez-Amor, M. Hydroxyapatite Coatings a Comparative Study between Plasma-Spray and Pulsed Laser Deposition Techniques. *J. Mater. Sci.: Mater. Med.* **1997**, *8*, 861−865.

(8) Wei, X.; Fu, C.; Savino, K.; Yates, M. Z. Carbonated Hydroxyapatite Coatings with Aligned Crystal Domains. *Cryst. Growth Des.* **2012**, *12*, 3474−3480.

(9) Roy, M.; Fielding, G. A.; Beyenal, H.; Bandyopadhyay, A.; Bone, S. Mechanical, in Vitro Antimicrobial, and Biological Properties of Plasma-Sprayed Silver-Doped Hydroxyapatite Coating. *ACS Appl. Mater. Interfaces* **2012**, *4*, 1341−1349.

(10) Terra, J.; Dourado, E. R.; Eon, J. G.; Ellis, D. E.; Gonzalez, G.; Rossi, A. M. The Structure of Strontium-Doped Hydroxyapatite: An Experimental and Theoretical study. *Phys. Chem. Chem. Phys.* **2009**, *11*, 568−577.

(11) Zhang, M. Y.; Cheng, G. J. Continuous Mode Laser Coating of Hydroxyapatite/ Titanium Nanoparticles on Metallic Implants: Multiphysics Simulation and Experimental Verification. *Trans. ASME, Ser. B* **2011**, *133*, 021010.

(12) Zhang, M. Y.; Cheng, G. J. Nanoscale Size Dependence on Pulsed Laser Sintering of Hydroxyapatite/Titanium Particles on Metal Implants. *J. Appl. Phys.* **2010**, *108*, 113112.

(13) Carradó, A. Structural, Microstructural, and Residual Stress Investigations of Plasma-Sprayed Hydroxyapatite on Ti-6Al-4V. *ACS Appl. Mater. Interfaces* **2010**, *2*, 561−565.

(14) Corno, M.; Rimola, A.; Bolis, V.; Ugliengo, P. Hydroxyapatite as a Key Biomaterial: Quantun-Mechanical Simulation of its Surfaces in Interaction with Biomolecules. *Phys. Chem. Chem. Phys.* **2010**, *12*, 6309−6329.

(15) Canepa, P.; Chiatti, F.; Corno, M.; Sakhno, Y.; Martra, G.; Ugliengo, P. Affinity of Hydroxyapatite (001) and (010) Surfaces to Formic and Alendronic Acids: A Quantum- Mechanical and Infrared Study. *Phys. Chem. Chem. Phys.* **2011**, *13*, 1099−1111.

(16) Khavryuchenko, V. D.; Khavryuchenko, O. V.; Lisnyak, V. V. Quantum Chemical Study of Water Impact on the Calcium Hydroxyapatite. *J. Phys.: Conf. Ser.* **2009**, *177*, 012005.

(17) Guo, T.; Zhou, S. B.; Zheng, X. T.; Jiang, J. Modeling and Investigation of Interfacial Interaction between PLA and One Type of Deficient Hydroxyapatite. *J. Phys. Chem. A* **2009**, *113*, 7112−7123.

(18) Lou, Z. Y.; Zeng, Q.; Chu, X.; Yang, F.; He, D. W.; Yang, M. L.; Xiang, M. L.; Zhang, X. D.; Fan, H. S. First-Principles Study of the Adsorption of Lysine on Hydroxyapatite (100) Surface. *Appl. Surf. Sci.* **2012**, *258*, 4911−4916.

(19) Almora-Barrios, N.; Austen, K. F.; de Leeuw, N. H. Density Functional Theory Study of the Binding of Glycine, Proline, and Hydroxyproline to the Hydroxyapatite (0001) and $(01\bar{1}0)$ Surfaces. *Langmuir* **2009**, *25*, 5018−5025.

(20) Almora-Barrios, N.; de Leeuw, N. H. Molecular Dynamics Simulation of the Early Stages of Nucleation of Hydroxyapatite at a Collagen Template. *Cryst. Growth Des.* **2012**, *12*, 756−763.

(21) Rimola, A.; Aschi, M.; Orlando, R.; Ugliengo, P. Does Adsorption at Hydroxyapatite Surfaces Induce Peptide Folding? Insights from Large-Scale B3LYP Calculations. *J. Am. Chem. Soc.* **2012**, *134*, 10899−10910.

(22) Almora-Barrios, N.; de Leeuw, N. H. A Density Functional Theory Study of the Interaction of Collagen Peptides with Hydroxyapatite Surfaces. *Langmuir* **2010**, *26*, 14535−14542.

(23) Chiatti, F.; Corno, M.; Ugliengo, P. Stability of the Dipolar (001) Surface of Hydroxyapatite. *J. Phys. Chem. C* **2012**, *116*, 6108−6114.

(24) Banerjea, A.; Smith, J. Origins of the Universal Binding-Energy Relation. *Phys. Rev. B* **1988**, *37*, 6632−6645.

(25) Kresse, G.; Furthmiiller, J. Efficient Iterative Schemes for Ab Initio Total-Energy Calculations Using a Plane-Wave Basis Set. *Phys. Rev. B* **1996**, *54*, 11169−11186.

(26) Kresse, G.; Hafner, J. Ab Initio Molecular Dynamics for Liquid Metals. *Phys. Rev. B* **1993**, *47*, 558−561.

(27) Perdew, P. J.; Burke, K.; Ernzerhof, M. Generalized Gradient Approximation Made Simple. *Phys. Rev. Lett.* **1996**, *77*, 3865−3868.

(28) Momma, K.; Izumi, F. VESTA 3 for Three-Dimensional Visualization of Crystal, Volumetric and Morphology Data. *J. Appl. Crystallogr.* **2011**, *44*, 1272−1276.

(29) Posner, A. S.; Perloff, A.; Diorio, A. F. Refinement of the Hydroxyapatite Structure. *Acta Crystallogr.* **1958**, *11*, 308−309.

(30) Rulis, P.; Ouyang, L. Z.; Ching, W. Y. Electronic Structure and Bonding in Calcium Apatite Crystals: Hydroxyapatite, Fluorapatite, Chlorapatite, and Bromapatite. *Phys. Rev. B* **2004**, *70*, 155104.

(31) Kim, J. Y.; Fenton, R. R.; Hunter, B. A.; Kennedy, B. Powder Diffraction Studies of Synthetic Calcium and Lead Apatites. *Aust. J. Chem.* **2000**, *53*, 679−686.

(32) de Leeuw, N. H. A Computer Modeling Study of the Uptake and Segregation of Fluoride Ions at the Hydrated Hydroxyapatite (0001) Surface: Introducing a $Ca_{10}(PO_4)_6(OH)_2$ Potential Model. *Phys. Chem. Chem. Phys.* **2004**, *6*, 1860−1866.

(33) Kittel, C. *Introduction to Solid State Physics*, 8th ed.; Johnson, S., Mcfadden, P., Smith, R., Lesure, M., Batey, M., Eds.; John Wiley & Sons, Inc: Hoboken, NJ, 2005; Chapter 1, p 20.

(34) Jahnátek, M.; Krajčí, M.; Hafner, J. Interatomic Bonding, Elastic Properties, and Ideal Strength of Transition Metal Aluminides: A Case Study for $Al_3(V,Ti)$. *Phys. Rev. B* **2005**, *71*, 024101.

(35) Sun, J. P.; Song, Y.; Wen, G. W.; Wang, Y.; Yang, R. Softening of Hydroxyapatite by Vacancies: A First Principles Investigation. *Mater. Sci. Eng., C* **2013**, *33*, 1109−1115.
(36) Fisher, E. S.; Renken, C. J. Single-Crystal Elastic Moduli and the Hcp→Bcc Transformation in Ti, Zr, and Hf. *Phys. Rev.* **1964**, *135*, 482−494.
(37) Huheey, J. E.; Keiter, E. A.; Keiter, R. L. *Principles of Structure and Reactivity: Inorganic Chemistry*, 4th ed.; Harper Collins College Publishers: New York, 1993.
(38) Snyders, R.; Music, D.; Sigumonrong, D.; Schelnberger, B.; Jensen, J.; Schneider, J. M. Experimental and Ab Initio Study of the Mechanical Properties of Hydroxyapatite. *Appl. Phys. Lett.* **2007**, *90*, 193902.
(39) Ching, W. Y.; Rulis, P.; Misra, A. Ab Initio Elastic Properties and Tensile Strength of Crystalline Hydroxyapatite. *Acta Biomater.* **2009**, *5*, 3067−3075.
(40) de Leeuw, N. H.; Rabone, J. A. L. Molecular Dynamics Simulations of the Interaction of Citric Acid with the Hydroxyapatite (0001) and (01$\bar{1}$0) Surfaces in an Aqueous Environment. *CrystEngComm* **2007**, *9*, 1178−1186.
(41) Christensen, A.; Carter, E. A. First-Principles Characterization of a Heteroceramic Interface: ZrO_2(001) Deposited on an α-Al_2O_3 (1$\bar{1}$02) Substrate. *Phys. Rev. B* **2000**, *62*, 16968.
(42) Christensen, A.; Jarvis, E. A. A.; Carter, E. A. In *Chemical Dynamics in Extreme Environments*; Dressler, R. A., Eds.; Advanced Series in Physical Chemistry; World Scientific: Singapore, 2001; Vol.*11*, pp 490.
(43) Forsgren, J.; Svahn, F.; Jarmar, T.; Engqvist, H. Formation and Adhesion of Biomimetic Hydroxyapatite Deposited on Titanium Substrates. *Acta Biomater.* **2007**, *3*, 980−984.
(44) Popov, M. N.; Spitaler, J.; Mühlbacher, M.; Water, C.; Keckes, J.; Mitterr, C.; Draxl, C. TiO_2(100)/Al_2O_3(0001) Interface: A First-Principles Study Supported by Experiment. *Phys. Rev. B* **2012**, *86*, 205309.
(45) Finnis, M. W. The Theory of Metal-Ceramic Interfaces. *J. Phys.: Condens. Matter* **1996**, *8*, 5811−5836.
(46) Hong, T.; Smith, J. R.; Srolovitz, D. J. Metal Ceramic Adhesion: A First Principles Study of MgO/Al and MgO/Ag. *J. Adhes. Sci. Technol.* **1994**, *8*, 837−851.
(47) Wang, F.; Li, K.; Zhou, N. G. First-Principles Calculations on Mg/Al_2CO Interfaces. *Appl. Surf. Sci.* **2013**, *285*, 879−884.
(48) Feng, N.; Mi, W. B.; Cheng, Y. C.; Guo, Z. B.; Schwingenschlögl, U.; Ba, H. L. Magnetism by Interfacial Hybridization and P-Type Doping of MoS_2 in Fe_4N/MoS_2 Superlattices: A First-Principles Study. *ACS Appl. Mater. Interfaces* **2014**, *6*, 4587−4594.
(49) Quintero, Y. C.; Ramanath, G.; Ramprasad, R. Environment-Dependent Interfacial Strength Using First Principles Thermodynamics: The Example of the Pt-HfO_2 Interface. *J. Appl. Phys.* **2013**, *114*, 163503.
(50) Jung, J.; Cho, M.; Zhou, M. Ab Initio Study of the Fracture Energy of $LiFePO_4$/$FePO_4$ Interfaces. *J. Power Sources* **2013**, *243*, 706−714.